ASCE
AMERICAN SOCIETY OF CIVIL ENGINEERS

Publications
Bruce Gossett, *Managing Director and Publisher*

Journals Department
Angela Cochran, *Director, Journals*
Kelly Anderson, *Managing Editor, Journals*
Holly Koppel, *Managing Editor, Journals*
Elizabeth Guertin, *Publishing Manager, Journals*
Jennifer Parresol, *Senior Editorial Coordinator*
Candice Gooch, *Editorial Coordinator*
Nick Violette, *Editorial Coordinator*

Production Department
Matt Boyle, *Director, Publications Production*
Michael Gentry, *Production Workflow Manager*
Rajashree Ranganathan, *Manager, Journals Production*
Heather DiAngelis, *Senior Production Editor*
Katie Fluke, *Production Editor*
DeAndréa Johnson, *Production Editor*
Patricia Jones Kershaw, *Production Editor*
Kathryn Doughty, *Production Coordinator*
Xi Van Fleet, *Senior Manager, Information Services*

Publishing Office
Journals Department
ASCE
1801 Alexander Bell Drive
Reston, VA 20191-4382
Telephone: (703) 295-6290
E-mail: journal-services@asce.org

Journal of Materials in Civil Engineering

VOLUME 27 / ISSUE 8 AUGUST 2015

SPECIAL SECTION: Asphalt Binder Characterization

SPECIAL SECTION EDITORS: YuZhen Zhang and Shin-Che Huang

Introduction

Technical Papers

Journal of
Materials in
Civil Engineering

VOLUME 27 / ISSUE 8
AUGUST 2015

OTHER ARTICLES

Technical Papers

Journal of
Materials in
Civil Engineering

VOLUME 27 / ISSUE 8
AUGUST 2015

Corrections

Evaporation from Porous Building Materials and Its Cooling Potential

Teresa Diaz Gonçalves, Ph.D.[1]; Vânia Brito[2]; Filipa Vidigal[3]; Luís Matias, Ph.D.[4]; and Paulina Faria, Ph.D.[5]

Abstract: Evaporative cooling is a traditional strategy to improve summer comfort, which has gained renewed relevance in the context of the transition to a greener economy. Here, the potential for evaporative cooling of common porous building materials, like natural stone and ceramic brick, is evaluated. The work has relevance also to the protection of built heritage because evaporation underlies the problems of dampness and salt crystallization, which are so harmful and frequent in this heritage. It was observed that the drying rate of the materials is, in some cases, higher than the evaporation rate of a free water surface. Surface area measurements by a three-dimensional optical technique suggested, as probable cause of this behavior, that surface irregularity gives rise to a large effective surface of evaporation in the material. Surface temperature measurements by infrared were performed afterward during evaporation experiments outside during a hot summer day in Lisbon. Their results indicate that ordinary building materials can be very efficient evaporative media and, thus, may help in achieving higher energy efficiency while maintaining a simultaneous constructive or architectural function. **DOI: 10.1061/(ASCE)MT.1943-5533.0001174.**

Author keywords: Porous media; Surface roughness; Fractals; Evaporation; Cooling.

Introduction

Water is a constant presence in the intricate pore network of traditional building materials, such as mortar, stone, or ceramics. It may have very harmful effects because it functions as a catalyst for deterioration mechanisms such as sulphate attack, biodeterioration, or salt decay. But it can also have positive effects, for example, when it enables the evaporative cooling of environments.

The evaporative drying of porous materials involves liquid transport toward an evaporation front and vapor transport from that front outward (Sherwood 1929; Scherer 1990). Two main regimes are in general considered, which for a material drying from saturation, correspond to the following main stages (Fig. 1): in Stage I, also called the constant drying rate period (CDRP), there is liquid continuity across the material and the wet front is located at their surface; the drying rate is constant because drying proceeds under steady-state conditions. Stage II, also called the falling drying rate period (FDRP), starts when the moisture content in the material, and therefore the liquid flow, decreases to a point where it is no longer able to compensate the evaporative demand and, therefore, the wet front recedes toward the interior of the material.

During the CDRP, the drying rate is at its highest value. This value is often assumed to be equal to that of a free water surface, which would be explained by the presence of a liquid film covering the whole surface of the material. However, this idea has been contradicted by researchers, such as Hammecker (1993), Jeannette (1997), Tournier et al. (2000), Rousset-Tournier (2001), and Diaz Gonçalves et al. (2012). These researchers observed that the evaporation rate from porous stones and other building materials during the CDRP was not necessarily equal to the evaporation from a free water surface and, in fact, could even be higher than that. A similar phenomenon was observed by Tang and Etzion (2004) who noticed that, with a low wind velocity, the rate of evaporation from a pond was greater when it was covered with wet tissue.

The possible enhancement of the CDRP drying rate of a porous material in comparison to a flat water surface has a wide range of implications. Indeed, evaporation is often used as a boundary condition in numerical models for moisture transport in porous media, and the most current reference for the CDRP is the evaporation rate of a flat water surface. The study of evaporative processes is also extremely important from more practical perspectives, such as the protection of the built heritage. The evaporation rate determines, for example, the height of capillary rise (I'Anson and Hoff 1984), a chronic problem in historical buildings (Massari and Massari 1993). Also, salt decay, one very harmful degradation mechanism that often affects this type of building (Charola 2000), happens precisely during evaporative processes (by which the solutions increase their concentration until they saturate and eventually crystallize). The study of evaporative drying is therefore fundamental to understand and ultimately develop solutions for these degradation processes. Finally, such study is also relevant from the point of view of sustainability because it is the base of evaporative cooling, one of the oldest strategies for improving summer comfort in hot, dry environments. The wetting of ceramic floors, traditional in Mediterranean countries, such as Portugal, can be mentioned as an example. Evaporative cooling methods rely on the fact that the passage of water from liquid to vapor state involves energy consumption (Matias et al. 2007). These cooling methods have recently gained a new importance and are more and more often

[1]National Laboratory for Civil Engineering (LNEC), Materials Dept., Av. do Brasil 101, 1700-066 Lisbon, Portugal (corresponding author). E-mail: teresag@lnec.pt

[2]National Laboratory for Civil Engineering (LNEC), Materials Dept., Av. do Brasil 101, 1700-066 Lisbon, Portugal. E-mail: vbrito@lnec.pt

[3]Dept. of Civil Engineering, LNEC and Nova Univ. of Lisbon, Caparica Campus, 2829-516 Caparica, Portugal. E-mail: filipavidigal@hotmail.com

[4]National Laboratory for Civil Engineering (LNEC), Buildings Dept., Av. do Brasil 101, 1700-066 Lisbon, Portugal. E-mail: lmatias@lnec.pt

[5]Nova Univ. of Lisbon, Dept. of Civil Engineering, Caparica Campus, 2829-516 Caparica, Portugal. E-mail: mpr@fct.unl.pt

Note. This manuscript was submitted on January 31, 2014; approved on August 5, 2014; published online on October 1, 2014. Discussion period open until March 1, 2015; separate discussions must be submitted for individual papers. This paper is part of the ***Journal of Materials in Civil Engineering***, © ASCE, ISSN 0899-1561/04014222(10)/$25.00.

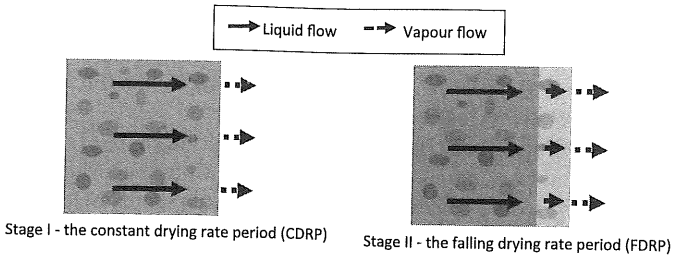

Fig. 1. A schematic representation of the two main drying stages of a porous material

incorporated in modern architectural solutions to help meet energy-efficiency needs.

In this study, the drying rate of porous building materials during the CDRP is experimentally analyzed. The objective was to investigate the possible enhancement of the CDRP drying rate in comparison to a flat water surface. To support the interpretation of the results, surface area measurements by a three-dimensional (3D) optical technique were carried out. Afterward, the evaporative cooling potential of some of the materials was assessed through the measurement of surface temperature with an infrared (IR) thermometer

Materials and Methods

Materials

The materials used for determination of the CDRP drying rate are rigid building materials that encompass six natural stones, a red ceramic brick, an air lime/sand mortar, and three calcium silicate materials (Table 1). They were chosen, on an exploratory basis, for being representative of those used in civil engineering and found in the built heritage and also because they cover a wide range of capillary porosity. Capillary porosity corresponds to the natural capacity of the material to absorb water at atmospheric pressure, and its values for the tested materials are also given in Table 1. The pore-size distribution of ten out of the eleven of the materials is presented in Fig. 2. An Autoscan60 porosimeter from Quantachrome was used, with a pressure range between 0 and 320 MPa. The measurements were performed according to ASTM D4404-10 standard (ASTM 2010) and were always replicated. The pore-size distribution of the remaining material, Maastricht limestone, can be found elsewhere (De Clercq et al. 2007). Incoherent materials like sand, sawdust, and cellulose, were also used, as reference, in the evaporative cooling tests (Table 2).

Measurement of CDRP Drying Rate

The CDRP drying rate was measured by means of drying tests (RILEM 1980). The method is similar to that described in Diaz Gonçalves et al. (2012) except that, here, the experiments lasted just long enough to measure the CDRP drying rate. They were carried out in a conditioned room at 20°C and 50% relative humidity (RH). To eliminate the influence of air velocity, the tests were carried out inside a box. This box is made of acrylic glass, has internal dimensions of 500 × 500 × 500 mm and possesses a 70-mm-diameter circular opening at the top to allow removing the specimens with minimal perturbation of the internal conditions. The RH inside the box was controlled by means of salts solutions, a desiccant, or simply by leaving it open (Table 3).

Table 1. Rigid Materials Used for Determination of the CDRP Drying Rate

Reference	Description	Capillary porosity[a] (%V)	
		Average	Standard deviation
CS.LS	Calcium silicate board PROMATECT—LS (Promat)	81.9	0.5
CS.L500	Calcium silicate board PROMATECT—L500 (Promat)	81.3	0.7
M	Maastricht limestone	42.7	1.2
MB	Malta Globigerina limestone—Badjda type	26.6	0.3
CS.B	Calcium silicate brick VB15 (Silka)	25.6	0.4
L	Lecce calcarenite	24.4	0.1
CA	Ançã limestone	22.8	0.7
A	Lime mortar (1:3 by volume of air lime and sand)	20.8	0.4
T	Solid red ceramic brick (Cerâmica Vale de Gândara, Portugal)	19.6	0.2
CB	Current Portuguese limestone of intermediate porosity	13.5	0.9
CC	Current Portuguese limestone of low porosity	9.1	0.1

[a]The capillary porosity was measured after complete immersion in water for 48 h, following RILEM procedure II.1 (RILEM 1980). Three specimens of each kind were used.

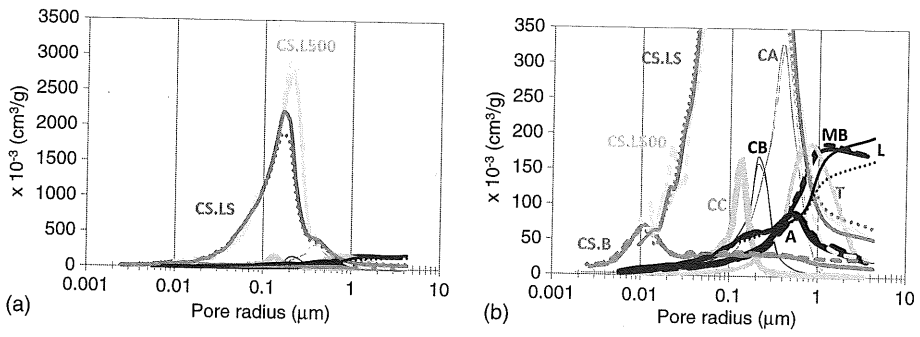

Fig. 2. Pore-size distribution as determined by mercury instrusion porosimetry (MIP)

Table 2. Incoherent Materials Used as Reference in Evaporative Cooling Tests

Reference	Description
AF	Fine siliceous sand 0.08–0.16 mm[a]
AM	Medium siliceous sand 0.30–0.50 mm[a]
AG	Coarse siliceous sand 1.60—2.00 mm[a]
S	Sawdust: residual material of a sawmill
C	Cellulose: paper paste from the paper industry; supplied by Portucel Soporcel

[a]According to EN 196-1 (CEN 2005).

Table 3. Environmental Conditions during Drying Experiments

	RH (%) at 20°C	
RH control	Nominal RH	Actual RH_{av}[a]
$CaCl_2$ (powder)	0.0[b]	25.2 ± 3.1
LiCl (saturated solution)	12.4[c]	44.4 ± 5.3
No salt (box left open)	50.0 (as in the lab room)	66.3 ± 2.0
NaCl (saturated solution)	75.5[c]	79.2 ± 3.5

[a]Average and standard deviation values of the actual RH in the box during the CDRP.
[b]Data from CEN (2001).
[c]Data from ASTM (2007).

The specimens were small cubes with 24-mm edge. The mortar cubes were made using metallic molds. The other specimens were sawed from larger stone blocks, ceramic bricks, and calcium silicate brick or insulation boards. All the cubes were brushed to remove as much stone or brick powder as possible from their surfaces. Then, they were cleaned in an ultrasonic cleaner (model B1200 E-1, Branson Ultrasonics Corporation). Finally, they were laterally sealed with epoxy.

For every condition, the materials and free water surfaces were tested simultaneously. The specimens were first saturated by partial immersion in pure water during three days. Afterward, their bottom surface was sealed with polyethylene (PE) film. They were then left to dry and were periodically weighted during 8 h.

Three test specimens of each kind of material were used at every condition, except for four of the materials, B, MB, CA, and T (Table 1). These materials had been previously tested and, therefore, it was considered reasonable to use only two specimens, as the preceding results were very homogeneous (Diaz Gonçalves et al. 2012). For the free water surfaces, three full petri dishes were always used.

The environmental conditions inside the drying box (Table 3) were continuously monitored by means of a Mikromec Multisens sensor positioned in its center. The measurements started before the specimens and petri dishes were placed inside the box and proceeded until after they were removed from it (Fig. 3). As seen both the initial RH and the final RH are similar to the nominal RH (Table 3). This means that when the wet materials and petri dishes are not inside the box, the actual RH (eventually) assumed the values expected in each case. The localized perturbations of the RH seen in Fig. 3 were due to the periodic opening of the box and removal of the specimens to weight them. The actual RH considered for this work was the average of the RH measured during the CDRP in each test: 25, 44, 66, and 79%, respectively (Table 3).

The result of a drying test is a graph depicting the mass of the specimens as function of time (Fig. 4). The drying rate of the specimen, in g/h, is the slope of the mass–time function. This value is then divided by the area of the top surface of the specimen to obtain the amount of water evaporated per unit area, in $g/(m^2\ h)$.

Measurement of Surface Area by Optical Method

The surface texture of ten materials (those in Table 1, except the Maastricht limestone) was studied using the 3D optical measuring instrument Talysurf CLI 1000, by Taylor Hobson. The instrument was equipped with a (noncontact) white light CLA gauge with a vertical range of 3 mm, vertical resolution of 100 nm, lateral resolution of 5 μm and measuring slope of 13° (Taylor Hobson 2009).

The measurements were carried out in 3D with the highest possible resolution, which corresponds to a spacing of 5 μm in both the X and Y directions. A velocity of 2 mm/s was chosen because it is the highest possible at the selected resolution.

Areal parameter Sdr (ISO 2012) was calculated after the measurements, using the *Talymap Gold* software. Sdr is the developed interfacial area ratio and expresses the percentage of additional surface area contributed by the texture, as compared to the projected area. Using the resampling operator of the *Talymap* software, Sdr could be calculated for different measurement scales: 5 μm (the original measurement step), 10, 20, 50, 100, and 200 μm. From

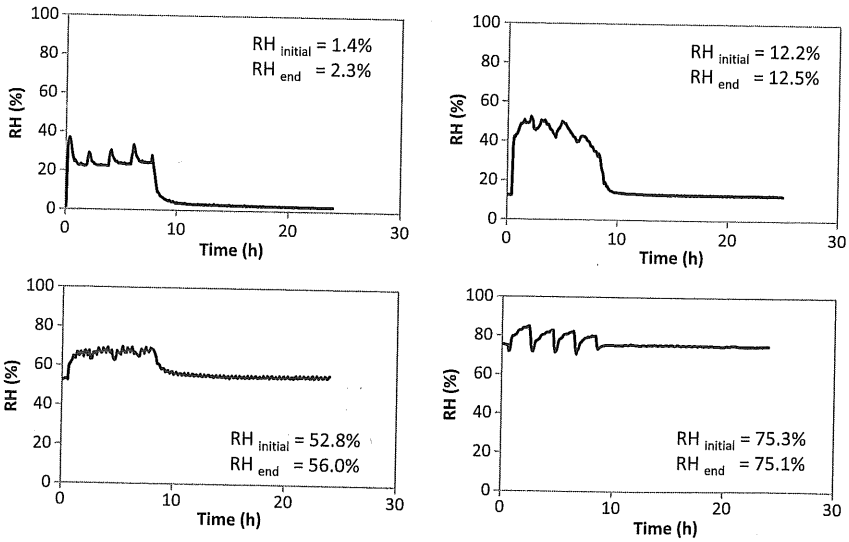

Fig. 3. RH inside the drying box during the experiments

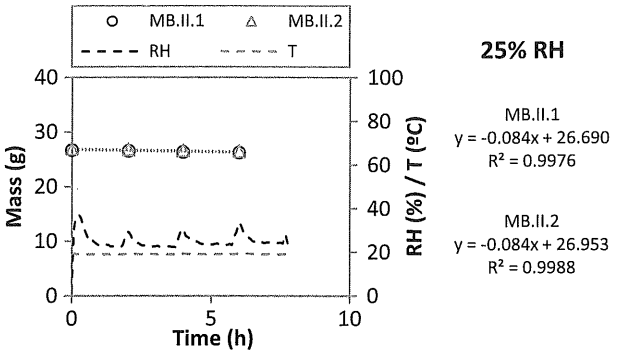

Fig. 4. Mass-time drying curves of two specimens of the MB stone, and environmental conditions (temperature and RH) during the test

the Sdr values, the relative area (RA) could be determined. RA is a dimensionless quantity that expresses the ratio between the projected surface area A of a material and its developed surface area [Eq. (1)]

$$RA = \frac{A_{\text{developed}}}{A_{\text{projected}}} = \frac{Sdr}{100} + 1 \tag{1}$$

Evaporative Cooling Experiments in Real Outdoor Conditions

The evaporation experiments were undertaken in real outdoor conditions during a hot summer day in Lisbon. One test was carried out under direct sunlight and another in the shade. There were no nearby buildings or heat sources in the location chosen for the test at the campus of the National Laboratory for Civil Engineering (LNEC). Surface temperature was measured with an IR thermometer Raytek (model MX4PG).

The tests were carried out on five rigid materials, namely calcium silicate CS.L500, limestones M and CB, lime mortar A, and red ceramic brick T (Table 1). Distilled water and incoherent materials (siliceous sands AG, AM and AF, sawdust S, and cellulose C) were also tested to serve as reference (Table 2).

Cubic specimens of the rigid materials were used with 50-mm edge. For the calcium silicate it was necessary to use samples with a lower height, 35 mm, owing to the dimensions of the original boards. The four lateral sides of the specimens were sealed with epoxy. The incoherent materials and water were placed in acrylic boxes with internal dimensions of 50 × 50 × 50 mm. The base of these boxes was perforated to allow capillary absorption, and a filter paper was put on the inside to avoid material loss.

The materials were soaked by capillary absorption through the base, by partial immersion in water for 48 h in a conditioned room (20°C and 50% RH). After this period, the samples were removed from immersion and its lower face immediately sealed with PE film to ensure that drying would be unidirectional, taking place only through the upper surface.

The cubes and containers were fit in openings cut in a XPS board with dimensions of 800 × 800 × 50 mm, as shown in Fig. 5. Two specimens of each material were used, one wet and one dry, as well as two containers (AD1 and AD2) filled with distilled water. The dry materials, which served as a reference for subsequent interpretation of the results, were previously dried in an oven during 24 h at 60°C, followed by 24 h in the conditioned room at 20°C and 50% RH. After fitting all the materials and containers in the XPS board, the assembly was wrapped in PE film to prevent evaporation. The assembly and a container with water were then transported and left in the selected place (in the sun) at 12 p.m. They remained in these conditions for 1 h to stabilize their temperature, after which the PE film was removed and the two acrylic containers filled with water.

The surface temperature measurements [Fig. 5(a)] began immediately and were repeated every 15 min for 1.5 h. Temperature was measured in the center of the top surface of the specimens, with the IR thermometer positioned perpendicularly and at a distance of 350 mm from this surface. The environmental conditions (temperature and RH) were evaluated with a digital thermohygrometer.

Assessment of the Emissivity

The IR thermometer measures the amount of energy (radiance E, in W/m^2) emitted by an object. Then, based on an emissivity value entered by the operator, it calculates the surface temperature of that object through Eq. (2) which is based on Stephan Boltzmann law (Matias 2012)

$$E = \varepsilon \sigma T^4 \tag{2}$$

In this equation, ε (dimensionless) = emissivity of the material, which represents the relation between the radiance of the body and that of a black body (body that absorbs all radiation); σ = Stefan-Boltzmann constant which takes an absolute value of 5.67×10^{-8} $W/(m^2 K^4)$; and T = temperature (K).

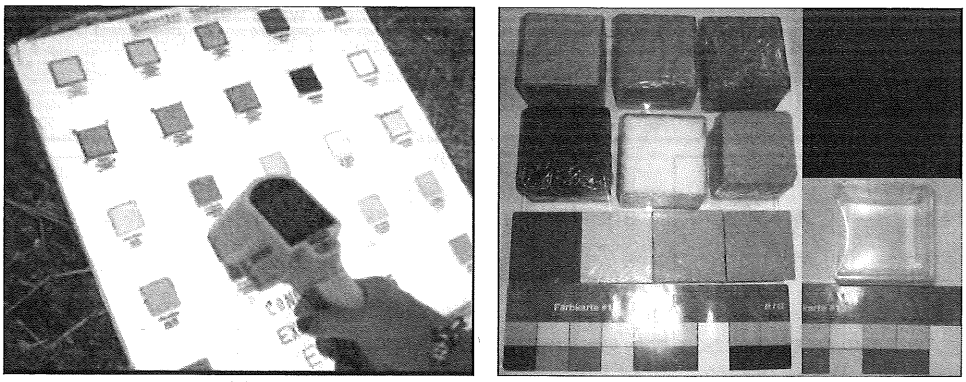

(a) (b)

Fig. 5. IR measurements of surface temperature: (a) measurement during one of the evaporative cooling experiments performed outdoors; (b) materials and water-filled container wrapped in PE film

Table 4. Some Emissivity Values Found in Literature

Materials	CONTEMP (2013)		FLIR (2008)		RAYTEK (2004)		Janssens (2003)	
	ε (−)	T(°C)	ε (−)	T(°C)	ε (−)	T(°C)	ε (−)	T(°C)
Calcium silicate	—	—	—	—	—	—	0.88	40–700
Limestone	0.30–0.40	—	—	—	0.98	25	—	—
Ceramic brick	0.93	20	0.81–0.86	17	0.90	25	—	—
Mortar	0.87	17	0.87	17	—	—	—	—
Sand	0.90	20	0.90	20	0.90	25	—	—
Wood	0.96	19	0.80–0.90[a]	20	0.94	25	—	—
White paper	0.93[b]	20	0.70-0.90	20	0.95	25	—	—
Distilled water	0.96	20	0.96	20	0.93[c]	25	—	—

[a]Wooden plates.
[b]Agglutinated.
[c]Water.

Table 5. Experimental Measurement of Emissivity

Materials	First test		Second test		
	Dry materials		Dry materials		Wet materials and water
	Without PE film	With PE film	Without PE film	With PE film	With PE film
AG	0.92	0.93	0.91	0.93	0.96
AM	0.92	**0.96**	0.90	0.93	0.96
AF	0.90	0.91	0.91	0.92	**0.97**
CS L500	0.93	0.92	0.85	0.90	0.95
T	0.94	0.92	0.85	0.91	0.93
A	**0.98**	0.92	**0.95**	**0.97**	**0.97**
CB	0.94	0.92	0.85	0.90	0.95
M	0.89	0.90	0.82	0.88	0.93
S	0.85	**0.88**	0.77	**0.87**	**0.92**
C	**0.84**	0.91	**0.80**	0.90	0.95
AD	—	—	—	—	**0.97**
Average	0.91	0.92	0.86	0.91	0.95[a]
Standard deviation	0.04	0.02	0.06	0.03	0.02[a]

Note: Boldface indicates the maximum and the minimum registered at each condition.
[a]Considering or not the distilled water.

For most of the tested materials and also for the water, emissivity values can be found in the literature (Table 4). These are, however, quite variable from author to author and sometimes given as a range rather than as individual values. Further, they always concern materials in the dry state.

Therefore, it was decided to measure experimentally the emissivity of the present materials and distilled water. This was carried out following the method recommended by the manufacturer of the IR thermometer. The specimens were first left in a conditioned room at 20°C and 50% RH for several days, so that they were in thermal equilibrium. Then, successive measurements of their surface temperature were performed with the IR thermometer, changing the emissivity until a surface temperature identical to that expected under thermal equilibrium conditions, i.e., 20°C (293.15 K) was achieved. The wet materials and the water-filled container were involved in PE film, as shown in Fig. 5(b), to prevent evaporation because this would lower their surface temperature.

Two sets of measurements were carried out; the results are shown in Table 5 and Fig. 6. As seen, average emissivity values between 0.86 and 0.95 were obtained, with a tendency for having higher values associated with the use of the PE film [Fig. 6(a)], and even higher values with the presence of water in the material [Fig. 6(b)]. The dispersion of results within each test was not very expressive, as seen by the standard deviation values presented in Table 5, which represent a maximum of 7% in relation to the average values.

However, the repeatability of this method for determining the emissivity was not good, as shown by Fig. 6(c). For this reason, it was decided to adopt a single emissivity value for all the materials (which in fact is the usual procedure). A value of 0.92 was chosen because it is close to the obtained experimental values and also to those found in the literature for this type of materials.

Results and Discussion

CDRP Drying Rate and Surface Area

Fig. 7 depicts the variation of the CDRP drying rate (DR) of the materials and water surfaces as a function of the RH_{av} which is the average of the actual RH values measured during the CDRP

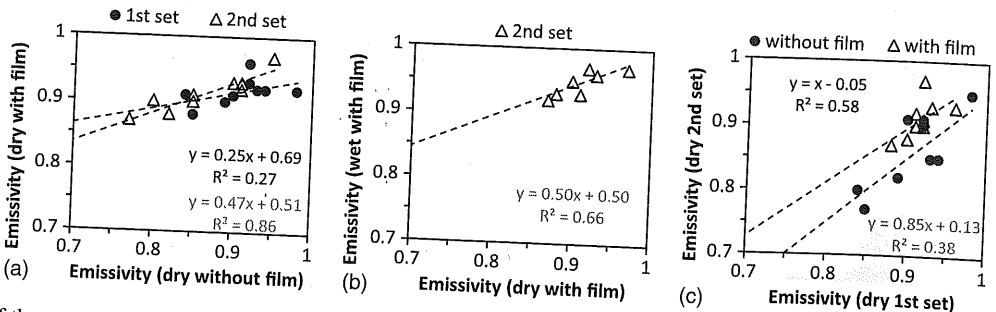

Fig. 6. Comparison of the measured emissivity values: (a) between materials with or without PE film; (b) between dry and wet materials; (c) among two identical tests on the same materials

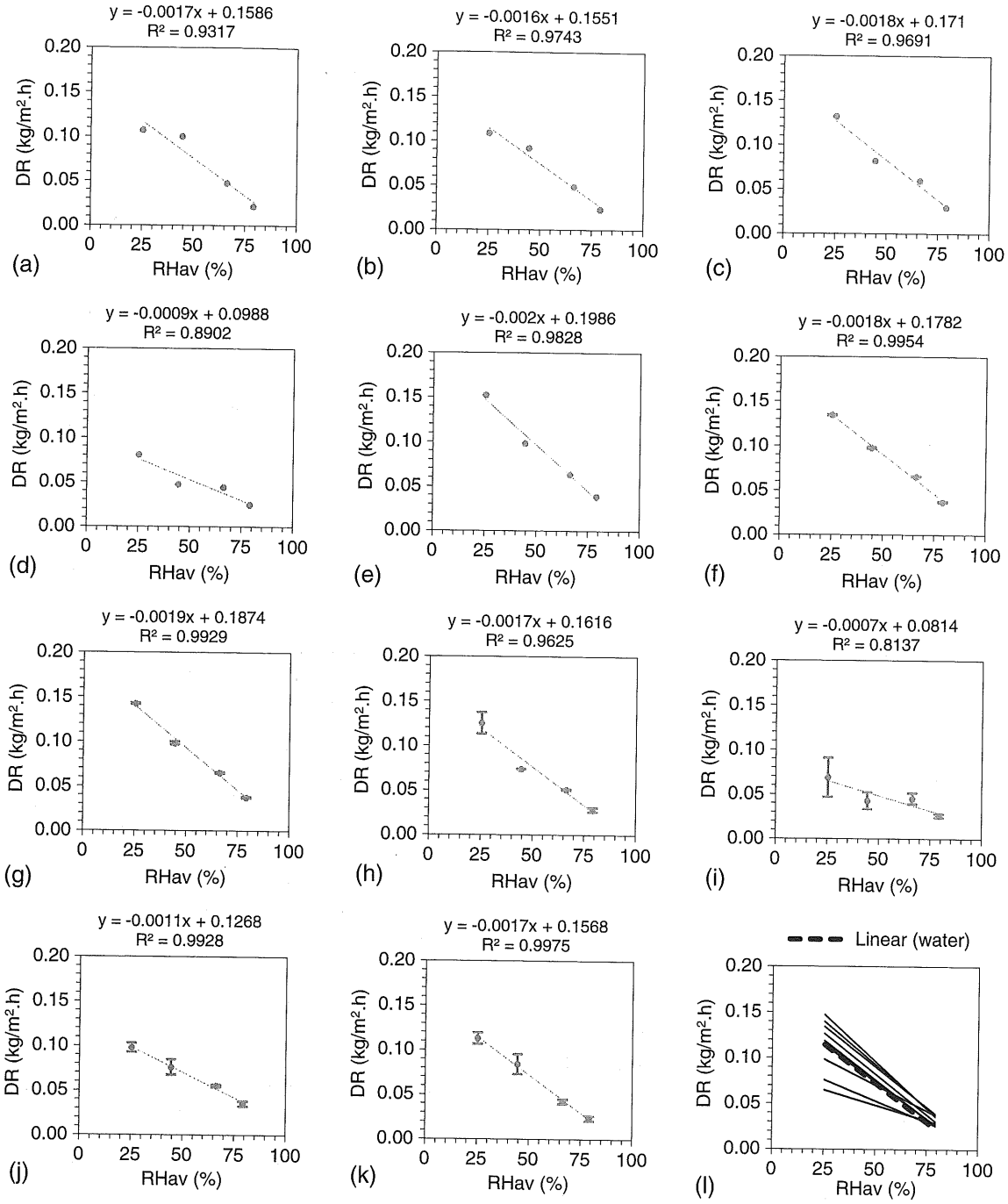

Fig. 7. Drying rate (DR) from materials during the CDRP and from free water surfaces as a function of the actual relative humidity (RH_{av}); the error bars correspond to one standard deviation above and one below the average: (a) CS.L500; (b) CS.LS; (c) CS.B; (d) A; (e) T; (f) CA; (g) MB; (h) L; (i) CC; (j) CB; (k) water; (l) all

(Table 3). As seen, the dispersion of the experimental values is low. The tendency to have slightly negative values of DR for RH = 100% in some cases suggests that the RH_{av} is a slight underestimate of the equivalent RH.

Despite these variation factors, there is an approximately linear relationship between the two quantities. This linearity means that Fick's law [Eq. (3)] is obeyed, which corresponds to an essentially diffusive process (Fig. 8). It also means that the thickness of the stagnant air layer δ adjacent to the material does not vary with the RH, which is likely to happen because the drying tests were performed within a closed box where, thus, air velocity was always close to zero

$$J = -\Pi \frac{dp}{dx} = -\frac{p_0}{100} \Pi \frac{d\mathrm{RH}}{dx} \tag{3}$$

where J ($ML^{-2}T^{-1}$) = mass flow of water vapor, i.e., the drying rate of the porous material; π (T) = vapor permeability of the layer that water vapor has to cross; dp/dx ($MT^{-2}L^{-2}$) = unidirectional vapor pressure gradient across that layer; and p_0 ($MT^{-2}L^{-1}$) = saturated vapor pressure.

Another relevant observation from Fig. 7 is that the CDRP drying rate of the materials is not necessarily equal to the evaporation rate from the free water surface tested under the same environmental conditions. It can be significantly lower, as it happens for example

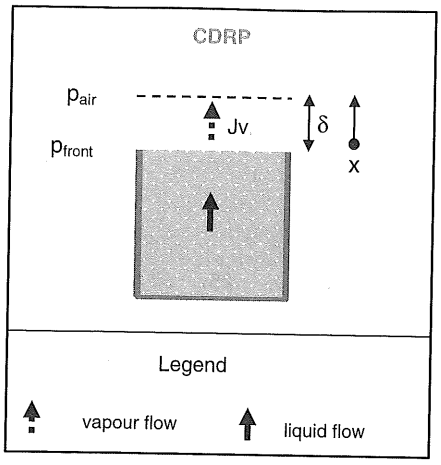

Fig. 8. Representation of CDRP as a diffusive process

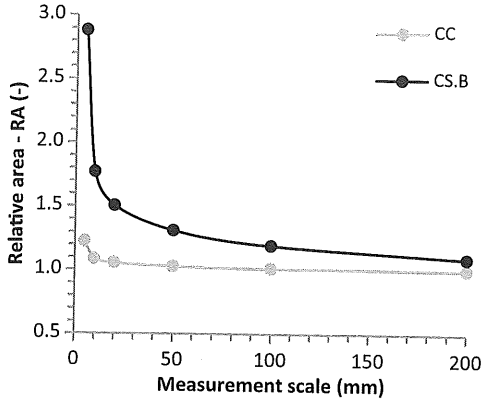

Fig. 9. Relative area (RA) of the surface of two CS.B and CC specimens as a function of the measurement scale

with the CC limestone in the majority of the conditions, but it can also be higher, as seen in Fig. 7(l). A CDPR drying rate higher than the evaporation rate from a free water surface had already been observed for different types of materials by several authors (Hammecker 1993; Jeannette 1997; Tournier et al. 2000; Rousset-Tournier 2001; Tang and Etzion 2004; Diaz Gonçalves et al. 2012).

The fact that in some cases the CDRP drying rate is lower than for a free water surface confirms that there is not a liquid film covering the total surface of the materials during the CDRP. If such a film existed, assuming that the liquid possesses the same thermodynamic properties in the pores and in a free surface, the drying rate of the material could perhaps be higher than for the free surface, due to surface irregularity, but it could never be lower.

Tournier et al. (2000) attributed the high CDRP drying rate of porous materials to their surface roughness. This broadly encompasses the fact that in the pores curved menisci are formed (rather than flat water surfaces), as well as the effect of the geometrical irregularity of the material surface.

However, the concept of (geometrical) surface roughness is questionable when applied to porous materials: straightforward extrapolation of what happens with other simpler types of surfaces, such as metals or plastics, is not possible. Table 6 depicts the values of the relative area obtained with the optical instrument at different scales, i.e., for different measuring steps. As seen, the RA values vary with the measurement scale. This variation of RA with the measurement scale is graphically depicted in Fig. 9 for the two materials (CS.B and CC) with the larger and smaller RA, respectively. These curves show that RA increases exponentially as the scale decreases, and that there is a vertical asymptote at point zero of the X-axis.

Table 6. Relative Area of Tested Material Surfaces at Different Measurement Scales (Average Values)

	Measurement scale (μm)					
Material	5	10	20	50	100	200
CS.LS	2.48	1.58	1.34	1.14	1.06	1.02
CS.L500	1.81	1.33	1.19	1.08	1.03	1.01
MB	1.69	1.28	1.19	1.12	1.06	1.02
CS.B	2.88	1.77	1.51	1.31	1.19	1.10
L	1.68	1.27	1.19	1.12	1.07	1.03
CA	1.22	1.08	1.06	1.03	1.02	1.01
A	2.33	1.59	1.37	1.26	1.23	1.17
T	1.29	1.12	1.07	1.03	1.02	1.01
CB	1.25	1.10	1.07	1.04	1.02	1.01
CC	1.22	1.09	1.05	1.03	1.01	1.00

These features indicate that the measured surfaces have fractal properties (Mandelbrot 1967, 1998). A fractal surface is an irregular surface with noninteger dimension between 2 (the Euclidian dimension of a plane) and 3 (the Euclidian dimension of a volume). Several authors have recognized and studied the fractal character of the pore space of natural and artificial porous building materials, such as natural stone (Katz and Thompson 1985; Bernal and Belo 2001), mortars (Arandigoyen et al. 2005; Arandigoyen and Alvarez 2006), or ceramic brick (Benavente et al. 2006). However, this concept has not yet been fully assimilated by civil engineering.

Due to the topological complexity of the pore space, a higher effective surface of evaporation is a likely explanation for the high CDRP drying rate depicted by some of the tested materials.

In Fig. 10, the CDRP drying rate is shown as a function of capillary porosity. Point (0,0) is attributed to a theoretical material with 0% porosity. Since it is admitted that surface irregularity derives from the presence of pores, this theoretical material would be totally flat. As can be seen in the figure, when the two calcium silicate materials with higher porosity are considered, the relationship between the CDRP drying rate and capillary porosity cannot be described by a linear function. Instead, a parabolic function may, for example, be used as a first-order approximation. This means that the CDRP drying rate will increase with increasing porosity but only up to a certain value. Any further rise in the porosity will result, rather, in a decrease of the drying rate. At a certain point, the situation of a free water surface is reached, which corresponds to the maximum possible porosity ($P = 1$). This behavior is consistent with the variation of the complexity of the physical surface (which is null for the two extremes ($P = 0$ and $P = 1$) and higher for the intermediate situations ($P \subset]0,1[$). However, it must also be noted that a clear correlation between the CDRP evaporation rate and the RA values measured with the profilometer was not found. The reason could be that RA varies with the measurement scale and the scale of interest is not necessarily the same for the different materials. Another possible reason could be that menisci curvature is also relevant in terms of effective surface of evaporation. These subjects clearly require further investigation.

Surface Temperature during Drying

Figs. 11 and 12 present the surface temperatures measured during the evaporation experiments performed outdoors, in the shadow and under the sun, respectively. The first observation is that the wet materials depict surface temperatures well below those of the dry materials, which is most likely due to the effect of evaporative cooling.

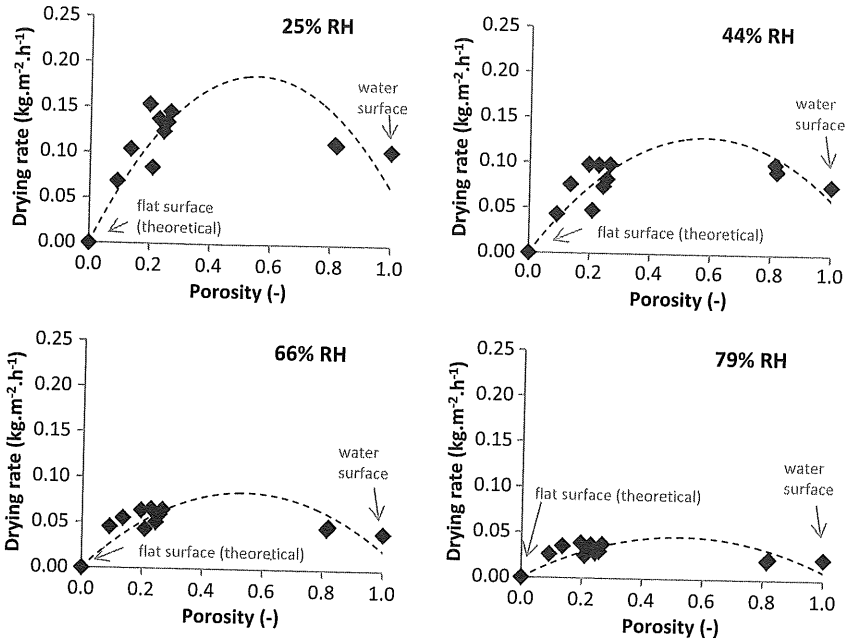

0. Variation of the CDRP evaporation rate with the capillary porosity. The free water surface is considered a material with 100% porosity; point is attributed to a theoretical material with 0% porosity

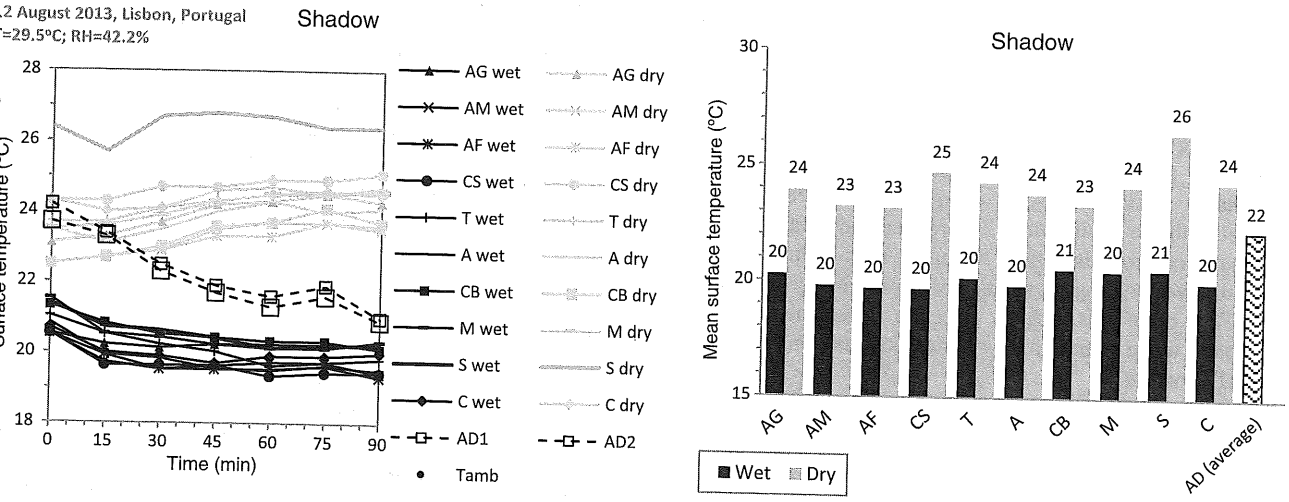

Fig. 11. Surface temperatures measured in shadow

ne shade (Fig. 11), the wet building materials achieve lower temperatures than the free water surface (AD) and depict no ant difference in relation to, for example, cellulose (C), s a product typically used in evaporative cooling devices. er the sun (Fig. 12), the situation is different. The brick (T), rse sand (AG), the mortar (A), and the sawdust (S) provide, case, surface temperatures of 1.2 to 6.3°C higher than the ter surface (AD). However, one of the limestones (M), ium silicate (CS), and two sands (AM and AF), achieve temperatures of 1.7 to 2.8°C lower than the free water surhough about 2.0°C to 3.1°C higher than cellulose (C). e results indicate, therefore, that ordinary building materi- interesting evaporative cooling potential. In the future, it e useful to investigate how much the heat capacity of the s and their coefficient of solar absorption contribute to the ces among them. It would also be important in the future to nore accurate emissivity data for the range of temperatures st, as emissivity may also depend on temperature. Such knowledge would allow developing a numerical model to support the proper development of evaporative cooling systems.

Conclusions and Perspectives

It was experimentally observed that the drying rate from porous building materials, such as natural stone or ceramic brick, can be very high during the CDRP. In some cases it may even overcome the evaporation rate from a free water surface subjected to similar environmental conditions. This high drying rate is probably due to the fractal character of the evaporating surface and possibly also to menisci curvature, as both features may enhance the effective surface of evaporation.

Due to their high CDRP drying rate, porous building materials have a high potential for evaporative cooling, which is in accordance with traditional uses in hot, dry climates, such as the wetting of ceramic tiles during summer in Mediterranean countries.

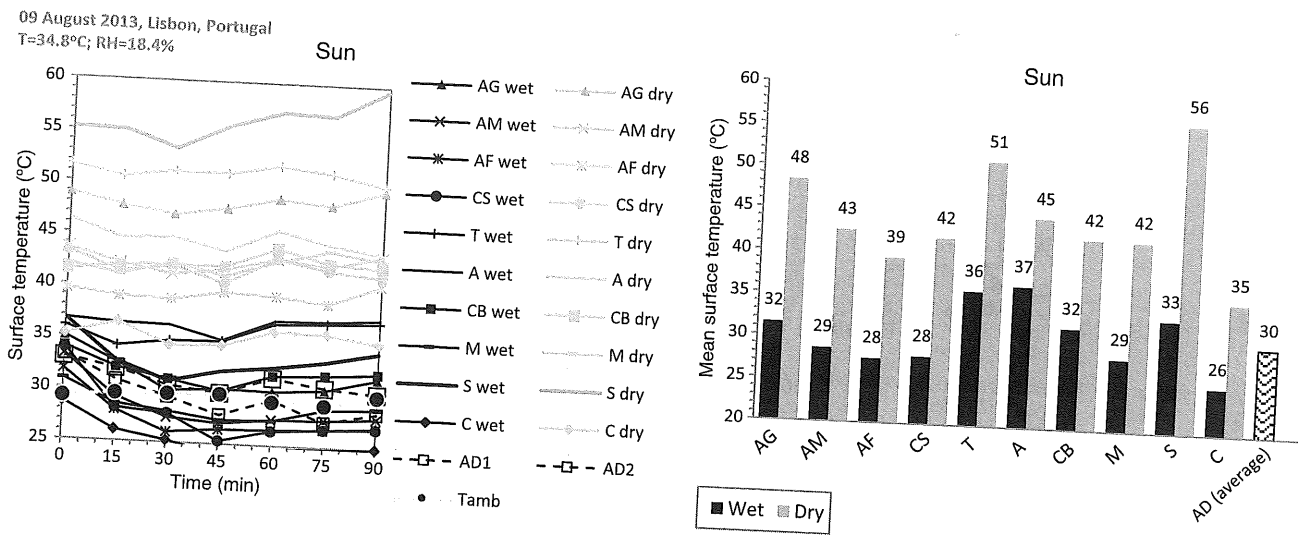

Fig. 12. Surface temperatures measured under the sun

This was confirmed experimentally, by means of evaporative cooling experiments performed in the exterior, during a hot summer day in Lisbon. The dry materials achieved high surface temperature, especially in the sun where some materials reached more than 50°C. However, during drying, their surface temperature dropped on average as much as 10 to 15°C. The surface temperature of the wet materials achieved values similar (in the sun) or even lower (in the shadow) than that of a free water surface.

This article is expected to contribute to a better assimilation by civil engineering disciplines of the idea that the surface morphology of ordinary porous building materials, such as brick or natural stone, has a fractal multiscale character that affects the way they interact with the environment. Moreover, the obtained experimental results confirm that these materials may be used in efficient evaporative cooling systems for low energy-consuming buildings. They may, thus, help to meet the current needs for energy efficiency while maintaining a simultaneous constructive or architectural function.

Acknowledgments

This work was funded by the Portuguese Foundation for Science and Technology (FCT) under the research project DRYMASS (ref. PTDC/ECM/100553/2008). Vânia Brito was supported by a research grant provided under this project. The authors are thankful to Leo Pel (TU/e) and José Delgado Rodrigues (LNEC) for their useful advice on different aspects of the study, and to LNEC technicians Luís Nunes and José Costa who helped on the experimental work. Thanks also to Jo Ann Cassar (University of Malta) for the Malta's Globigerina limestone, to Cerâmica do Vale de Gândara for the red ceramic brick, to Cristovão Soares (Tria) for the calcium silicate boards, to James Diamond (Ytong) for the calcium silicate bricks, to José Cruz (Lusical) for the dry hydrated lime, to Patricia Castellano Rodrigues (Portucel Soporcel) for the paper paste, and to Pedro Teixeira for his help with the contacts.

References

Arandigoyen, M., and Alvarez, J. I. (2006). "Blended pastes of cement and lime: Pore structure and capillary porosity." *Appl. Surf. Sci.*, 252(23), 7562–7571.

Arandigoyen, M., Pérez Bernal, J. L., Bello López, M. A., and Alvarez, J. I. (2005). "Lime-pastes with different kneading water: Pore structure and capillary porosity." *Appl. Surf. Sci.*, 252(5), 1449–1459.

ASTM. (2007). "Standard practice for maintaining constant relative humidity by means of aqueous solutions." *E104–02*, West Conshohocken, PA.

ASTM. (2010). "Test method for determination of pore volume and pore volume distribution of soil and rock by mercury intrusion porosimetry." *D4404-10*, West Conshohocken, PA.

Benavente, D., Linares-Fernández, L., Cultrone, G., and Sebastián, E. (2006). "Influence of microstructure on the resistance to salt crystallisation damage in brick." *Mater. Struct.*, 39(1), 105–113.

Bernal, J. L. P., and Bello, M. A. (2001). "Fractal geometry and mercury porosimetry comparison and application of proposed models on building stones." *Appl. Surf. Sci.*, 185(1–2), 99–107.

CEN. (2001). "Hygrothermal performance of building materials and products—Determination of water vapour transmission properties." *EN ISO 12572:2001*, Brussels, Belgium.

CEN. (2005). "Methods of testing cement—Part 1: Determination of strength." *CSN EN 196-1*, Brussels, Belgium.

Charola, A. E. (2000). "Salts in the deterioration of porous materials: An overview." *J. Am. Inst. Conserv.*, 39(3), 327–343.

CONTEMP. (2013). "Annexe: Emissivity tables." ⟨http://www.contemp.com.br/downloads/pdf/Tabela_de_Emissividades.pdf⟩ (Sep. 16, 2013).

De Clercq, H., De Zanche, S., and Biscontin, G. (2007). "TEOS and time: The influence of application schedules on the effectiveness of ethyl silicate based consolidants." *Restor. Build. Monuments*, 13(5), 305–318.

Diaz Gonçalves, T., Brito, V., and Pel, L. (2012). "Water vapor emission from rigid mesoporous materials during the constant drying rate period." *Dry. Technol.*, 30(5), 462–474.

FLIR Systems. (2008). "FLIR reporter professional. User's manual." ⟨http://support.flir.com/DocDownload/Assets/46/English/1558567$a269.pdf⟩ (Sep. 15, 2014).

Hammecker, C. (1993). "Importance of water transport in stone degradation in the field." Thèse de doctorat, Université Louis Pasteur, Strasbourg, France.

I'Anson, S. J., and Hoff, W. D. (1984). "Water movement in porous building materials—VIII. Effects of evaporative drying on height of capillary rise equilibrium in walls." *Build. Environ.*, 21(3–4), 195–200.

ISO. (2012). "Geometrical product specifications (GPS). Surface texture: Areal—Part 2: Terms, definitions and surface texture parameters." *ISO 25178–2*, Geneva.

Janssens, M. (2003). "Improved method for analyzing ignition data from the cone calorimeter in the vertical orientation." *Proc., 7th Int. Symp. Fire Safety Science*, MD.

Jeannette, D. (1997). "Structures of porosity, solutions transport mechanisms, and main alterations of rocks in monuments." *La Pietra dei*

Monumenti in Ambiente Fisico e Culturale, R. A. Lefèvre, ed., European Univ. Centre for Cultural Heritage, Ravello, Italy, 49–77.
Katz, A. J., and Thompson, A. H. (1985). "Fractal sandstone pores: Implications for conductivity and pore formation." *Phys. Rev. Lett.*, 54(12), 1325–1328.
Mandelbrot, B. (1967). "How long is the coast of Britain? Statistical self-similarity and fractional dimension." *Science*, 156(3775), 636–638.
Mandelbrot, B. (1998). *Fractal objects*, Gradiva, Lisboa, Portugal.
Massari, G., and Massari, I. (1993). *Damp buildings: Old and new*, ICCROM, Rome.
Matias, L. (2012). "Thermography." *Testing techniques for structures inspection*, Duratinet Course, LNEC, Lisbon, Portugal.
Matias, L., Vilhena, A., Cristian, A., Santos, C., and Veiga, M. (2007). "Laboratory thermographic analysis of masonry specimens. Capillarity and drying." *Proc., 7th Int. Symp. Conservation of Monuments in the Mediterranean Basin*, UNESCO World Heritage Centre (WHC), France.
RAYTEK. (2004). "High performance infrared thermometer." ⟨http://www.instrumart.com/assets/MX4_manual.pdf⟩ (Sep. 16, 2013).
RILEM TC 25-PEM. (1980). "Recommended tests to measure the deterioration of stone and to assess the effectiveness of treatment methods." *Mater. Struct.*, 13(75), 175–253.
Rousset-Tournier, B. (2001). "Transport by capillary action and evaporation in rocks. The role of porosity structures." Thèse de doctorat, Université Louis Pasteur, Strasbourg, France.
Scherer, G. W. (1990). "Theory of drying." *J. Am. Ceram. Soc.*, 73(1), 3–14.
Sherwood, T. K. (1929). "The drying of solids II." *Ind. Eng. Chem.*, 21(10), 976–980.
Talymap. Gold version 5.1.1 [Computer software]. Taylor Hobson.
Tang, R., and Etzion, Y. (2004). "Comparative studies on the water evaporation rate from a wetted surface and that from a free water surface." *Build. Environ.*, 39(1), 77–86.
Taylor Hobson. (2009). "Talysurf CLI: 3D surface profiling systems." ⟨http://www.f-di.hu/cli_systems.pdf⟩ (Nov. 13, 2013).
Tournier, B., Jeannette, D., and Destrigneville, C. (2000). "Stone drying: An approach of the effective evaporating surface area." *Proc., 9th Int. Congress on Deterioration and Conservation of Stone*, Elsevier, Amesterdam, Netherlands.